Stem Cell Reports
Report
ISSCR
OPEN ACCESS

Transplantation of human pluripotent stem cell-derived retinal sheet in a primate model of macular hole

Yasuaki Iwama,[1,2,3] Yasuko Sugase-Miyamoto,[4] Kenta Onoue,[5] Hirofumi Uyama,[1,2] Keiji Matsuda,[4] Kazuko Hayashi,[4] Ryutaro Akiba,[1] Tomohiro Masuda,[1,2] Satoshi Yokota,[1,2] Shigenobu Yonemura,[5,6] Kohji Nishida,[3] Masayo Takahashi,[1,2] Yasuo Kurimoto,[1,2] and Michiko Mandai[1,2,7,*]

[1]Laboratory for Retinal Regeneration, RIKEN Center for Biosystems Dynamics Research, Kobe, Hyogo 650-0047, Japan
[2]Kobe City Eye Hospital, Kobe, Hyogo 650-0047, Japan
[3]Department of Ophthalmology, Osaka University Graduate School of Medicine, Osaka 565-0871, Japan
[4]Human Informatics and Interaction Research Institute, National Institute of Advanced Industrial Science and Technology, Tsukuba 305-8568, Japan
[5]Laboratory for Ultrastructural Research, RIKEN Center for Biosystems Dynamics Research, Kobe, Hyogo 650-0047, Japan
[6]Department of Cell Biology, Tokushima University Graduate School of Medicine, Tokushima 770-8503, Japan
[7]Lead contact
*Correspondence: e_lab.mandai@kcho.jp
https://doi.org/10.1016/j.stemcr.2024.09.002

SUMMARY

Macular hole (MH) is a retinal break involving the fovea that causes impaired vision. Although advances in vitreoretinal surgical techniques achieve >90% MH closure rate, refractory cases still exist. For such cases, autologous retinal transplantation is an optional therapy showing good anatomic success, but visual improvement is limited and peripheral visual field defects are inevitable after graft harvesting. Here, using a non-human primate model, we evaluated whether human embryonic stem cell-derived retinal organoid (RO) sheet transplantation can be an effective option for treating MH. After transplantation, MH was successfully closed by continuous filling of the MH space with the RO sheet, resulting in improved visual function, although no host-graft synaptic connections were confirmed. Mild xenotransplantation rejection was controlled by additional focal steroid injections and rod/cone photoreceptors developed in the graft. Overall, our findings suggest pluripotent stem cell-derived RO sheet transplantation as a practical option for refractory MH treatment.

INTRODUCTION

Macular hole (MH) is a retinal break involving the fovea, which causes impaired vision including distortion and/or defect in central vision, and most often occurs in the elderly and females (McCannel et al., 2009). Tangential vitreomacular traction is considered as the major cause of MH (Gass, 1995). In the past decade, pars plana vitrectomy (PPV) with internal limiting membrane (ILM) peeling and gas tamponade became a standard procedure worldwide, with the initial closure rate of MH reaching >90% (Spiteri Cornish et al., 2014). However, refractory cases occur with conditions such as high myopia (Suda et al., 2011; Morgan et al., 2012) and large/chronic MHs (Ch'ng et al., 2018). Surgical management of recurrent MHs after primary surgery is also challenging (Frisina et al., 2022; Lorenzi et al., 2022), particularly when the ILM over the foveal area has been removed.

In such difficult cases, additional surgical techniques including lens capsular flap transplantation (Chen and Yang, 2016), free ILM flap transplantation (Morizane et al., 2014), human amniotic membrane transplantation (Rizzo et al., 2019), and autologous retinal transplantation (ART) (Grewal et al., 2019) can be used to increase the MH closure rate. Among them, ART shows good anatomical success (Frisina et al., 2022; Lorenzi et al., 2022) and has advantages such as graft vascularization continuous from the host retina (Tabandeh, 2020) and potential graft function in visual processing by contacting the host retina. However, as ART requires harvest of the transplant sheet in the peripheral retina, visual field defects at the harvested site are inevitable. Additionally, ART grafts from the peripheral retina are dominant in rod photoreceptor (PR) cells in contrast to the cone-dominant foveal part (Hendrickson et al., 2012), and how rod PRs are integrated in the foveal area remains unclear.

For retinal degenerative diseases, cell-based therapy is a promising strategy for restoring visual function in retinal degenerative diseases (Singh et al., 2013; Mandai et al., 2017; Gasparini et al., 2019; Ribeiro et al., 2021). We previously transplanted human embryonic stem cell (ESC)/induced pluripotent stem cell (PSC)-derived retinal organoid (RO) sheets in retinal degeneration animal models and observed maturation of graft PRs, potential host-graft synaptic connections, host retinal ganglion cell (RGC) responses to light in the grafted area, and functional improvements in visual field tests (Shirai et al., 2016; Tu et al., 2019; Yamasaki et al., 2022). In primate models, human PSC-derived RO sheets are considered to be useful as long-term graft survival has been confirmed (Tu et al., 2019). Additionally, we proved the enhanced functional integration of graft PRs and host secondary neurons using ISL1$^{-/-}$human embryonic stem cell (hESC)-derived RO sheets, genetically modified grafts lacking ON-bipolar cells

(BPs) while retaining functional PRs, in rodent models (Yamasaki et al., 2022). This strategy may also be beneficial in refractory MH cases; therefore, we evaluated whether an ISL1$^{-/-}$ hESC-derived RO sheet transplantation could be used to treat MH with the eye of a Japanese Macaque with MH associated with ILM peeling, which mimics refractory MH.

RESULTS

hESC-derived retinal transplantation in an MH model monkey

We prepared the Japanese Macaque as a primate model with possible MH (see supplemental experimental procedures) and observed both functional and anatomical outcomes after hESC-derived retinal transplantation. The monkey was referred to our laboratory upon discovery of bilateral MH by fundus examination at the National Institute of Advanced Industrial Science and Technology (AIST) in 2019 (Figure 1A). The monkey was transferred to our facility in 2021. Optical coherence tomography (OCT) revealed an outer nuclear layer (ONL) defect at the size of approximately 410- and <100-μm diameter with superficial connectivity on the top on the right and left eyes, respectively (Figure 1B). This monkey had no history associated with traumatic or toxic retinal damage. We considered the aforementioned etiology as spontaneous closure of MH (Garg et al., 2022) or macular degeneration, the cause of which is unknown, because fundus autofluorescence (FAF) showed a slightly hyperreflective area consistent with fovea and fluorescein angiography (FA) showed no abnormality (Figures 1C and 1D, respectively). We planned to transplant the hESC-derived RO sheet into the subretinal space of the right eye because this eye lacked ONL at the fovea; the left eye was followed without intervention because ONL disruption at the fovea was very small, which subsequently improved (Figure S1).

Because foveal retina is dominantly composed of PRs with radially extending axons toward the foveal margins where BPs align, we used a retinal sheet from a genetically modified Islet1$^{-/-}$ Crx::Venus hESC cell line (hESC-KhES-1), which was labeled for PRs and lacked ON-BPs (Figures 1E–1G) (Yamasaki et al., 2022). Although ILM peeling was gently performed after removing a sticky posterior vitreous cortex, intraoperative OCT demonstrated that the MH was open with a minimum diameter of around 330 μm (left, Figure 1H). We prepared hESC-derived RO sheets of around differentiation days (DD) 60, as done in our previous studies (Shirai et al., 2016; Yamasaki et al., 2022), with different sizes and inserted the appropriate one by tucking the edge under the host MH space margin to fill the open space (See Video S1). The surgery was finished with fluid-air exchange and sub-tenon steroid injection. We did not use silicon oil tamponade because intraoperative OCT (right, Figure 1H) revealed that the graft looked fixated under the retina in the whole circumference of the MH.

Anatomical closure of MH and mild rejection response to the retinal graft

One month after surgery, the hyperreflective retinal graft filled in the MH in the OCT image (Figure 2A). Until 3 months after transplantation, no rejection was observed in FA/OCT, and Crx::Venus-positive tissue, which has an excitation peak at 515 nm, was observed under the excitation lights of FA and FAF imaging, indicating the presence of maturing PRs. We administered cyclosporine orally with food to the monkey from 1 week before surgery. Although blood levels of cyclosporine were insufficient, we continued at the initial dose (20 mg/kg) because increasing the dose markedly decreased food intake. Four months after surgery, inner retinal fluids in the host parafovea and transient graft elevation with hyperreflectivity were observed by OCT; the Venus-positive area had shrunk in FA/FAF, although no obvious rejection responses to the graft, such as vascular leakage, were observed in FA (Figure 2B). Based on these results, we suspected a mild rejection response to the graft and conducted a sub-tenon steroid injection. Two weeks after steroid injection, the retinal edema was resolved with no recurrence until 6 months after surgery (Figure 2C). We conducted preventive sub-tenon steroid injection at 6 months after surgery to prevent further immune responses.

hESC-derived retinal tissue showed improvements in eye fixation test and electrophysiological response

A fixation test of each eye (Figures 3A and 3B) was performed in September 2019 with very low correct ratios of 1.5% (7/461) and 12.8% (130/1,013) for the right and left eyes, respectively (window size: 4° by 4°). After surgery, the same fixation tests were conducted on February 15–17, 2022. Invisible eye windows (Figure 3C) were set at 8° by 8°, and postoperative results were calculated under the same conditions as used preoperatively (4° by 4°). Compared with that before surgery, the correct ratio was significantly increased on all testing days after surgery (Figure 3D, $p < 0.0001$, Pearson's chi-squared test against correct/error trials before surgery, R version 3.1.0 [R Development Core Team, 2014]). This increase in the correct ratio on the left eye (non-transplanted eye) could be explained by a spontaneous recovery of the foveal structure (Figure S1). In Figure 3E, the position of the right eye across time was aligned for day 1 (February 15, 2022). Forty five out of 102 trials (red lines, Figure 3E) were distributed between −4° and 4° from the screen center.

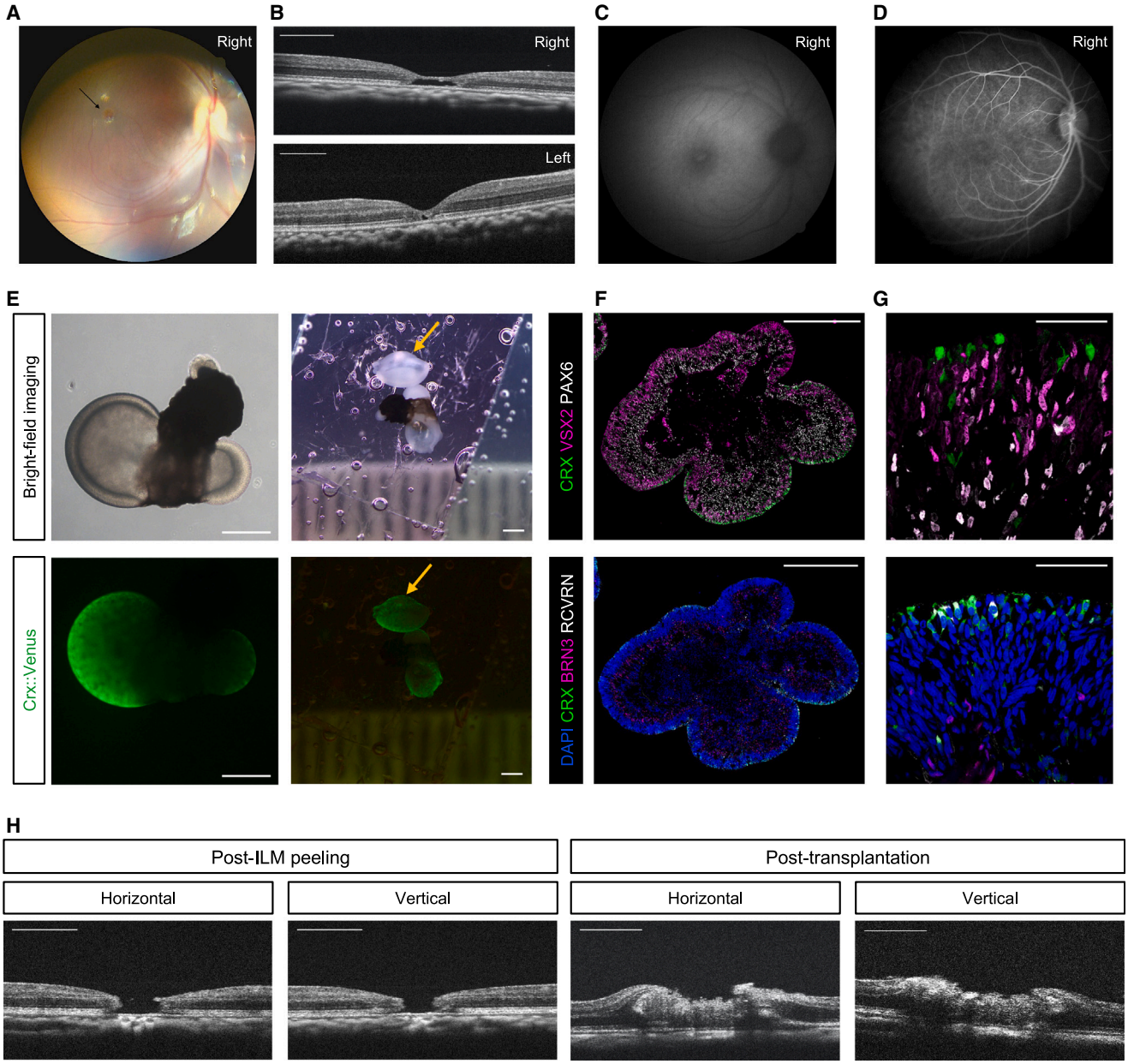

Figure 1. Macular hole model monkey, human embryonic stem cell-derived retinal graft, and intraoperative surgical procedures

(A–D) Preoperative conditions of the foveal area. Fundus photograph (A) was taken in 2019. Optical coherence tomography (OCT) (B), fundus autofluorescence (FAF) (C), and fluorescein angiography (FA) images at the early phase (D) were taken one week before surgery.

(E) Bright-field image (top) and Venus-fluorescent image (bottom) of Islet1$^{-/-}$ Crx::Venus retinal organoids (left) and retinal graft for transplantation (right).

(F and G) Immunostaining images of representative retinal organoids of the same batch as the graft on around DD60 with low and high magnification, respectively. PAX6 (white, top) and BRN3 (magenta, bottom; retinal ganglion cell marker) were expressed on the basal side, whereas VSX2 (magenta, top), RCVRN (white, bottom; photoreceptor marker), and CRX (green; photoreceptor marker) were expressed mainly on the apical side.

(H) Intraoperative OCT image of the foveal area after gentle ILM peeling (left) and retinal transplantation to the MH space (right). Scale bars: 500 μm (E), 200 μm (B, F, and H), and 50 μm (G).

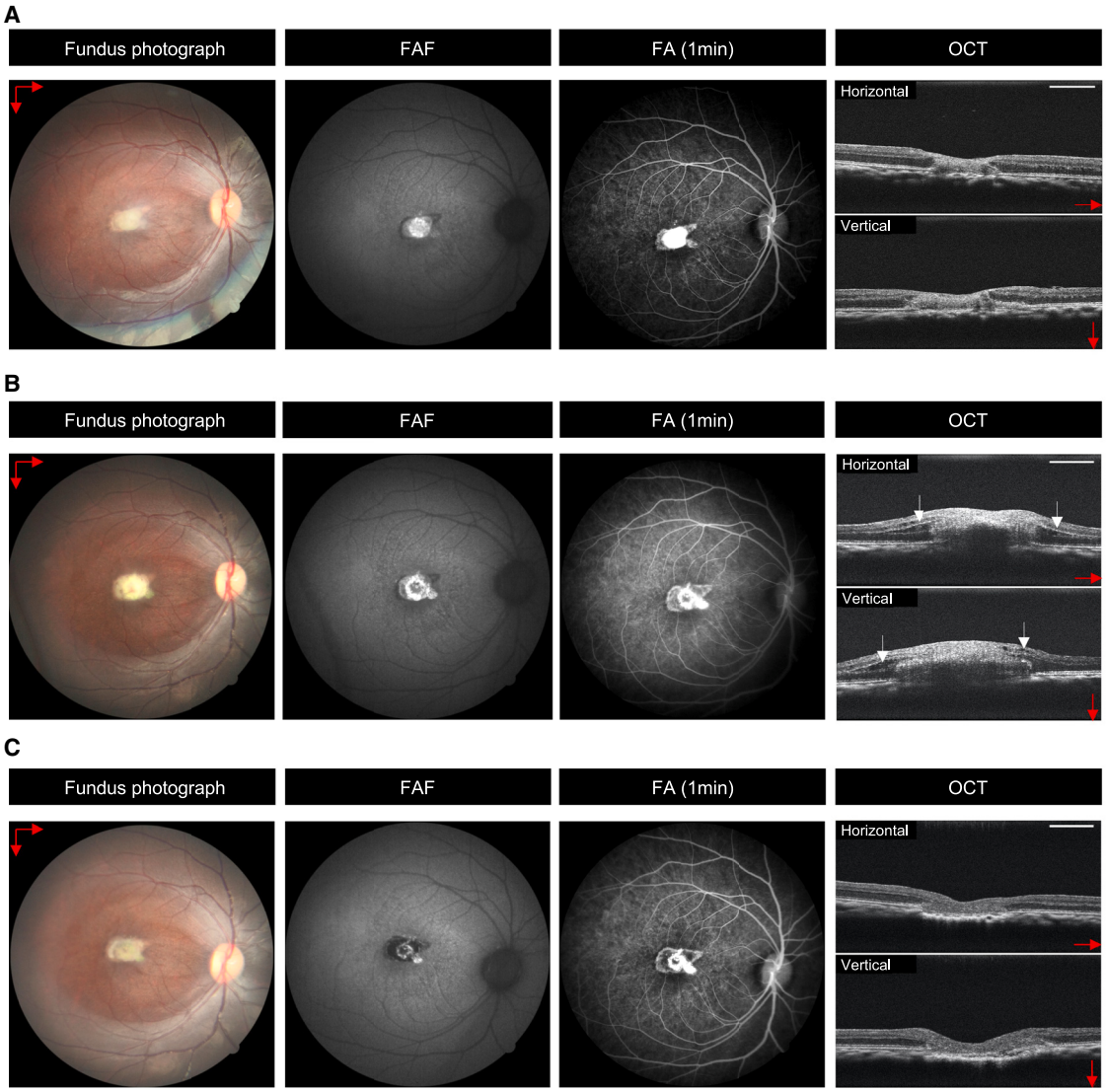

Figure 2. *In vivo* objective ophthalmic examinations after retinal transplantation to macular hole model monkey

(A–C) Fundus photographs, fundus autofluorescence (FAF) image, and fluorescein angiography (FA) image at the early phase, and optical coherence tomography (OCT) images of the foveal area at 1, 4, and 6 months after transplantation, respectively. Crx::Venus fluorescence can be observed in FAF and FA images. Red arrows in OCT images correspond to arrow directions, horizontal and vertical, on the fundus photographs.

(B) At 4 months after transplantation, inner retinal fluids were observed around the graft (white arrows).

(C) At 6 months after transplantation, inner retinal fluids around the graft were resolved after steroid injection. Scale bars: 500 μm (A–C).

We also recorded focal macular electroretinograms (ERGs) using the 200 times averaging of 5° spot stimulation before and 6–7 months after surgery (Figure 3F). Focal macular ERGs were recorded on the left eye as a positive control (right, Figure 3F). The b-wave amplitude was determined as the amplitude from the trough of the a-wave to the peak of the b-wave (Terasaki et al., 1998). The amplitude of the a-wave (white arrow, Figure 3F) was small and showed no remarkable differences before and after transplantation (0.47 vs. 0.40 μV, respectively). The b-wave amplitude (black arrow, Figure 3F) increased from 0.43 μV before surgery to 0.70 μV at 6 months after surgery; in contrast, the b-wave amplitude of the positive control was 1.01 μV.

hESC-derived retinal tissue showed graft survival and maturation and a mild immunological response in an MH model monkey

We performed immunohistochemical (IHC) evaluation and electron microscope (EM) analysis to evaluate the

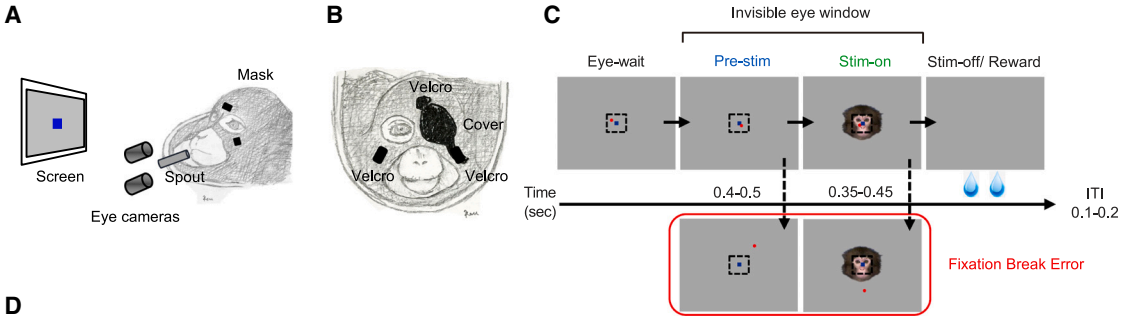

D

Eye open	Correct ratio % (number of correct/total trials)			
	Before surgery 9/24/2019	After surgery 2/15-17/2022		
		Day 1	Day 2	Day 3
Right	1.5 (7/461)	25.9 (45/174)***	10.9 (34/313)***	14.7 (27/184)***
Left	12.8 (130/1013)	54.0 (68/126)***	26.0 (51/196)***	46.2 (54/117)***

***: p < 0.0001, Pearson's Chi-squared test

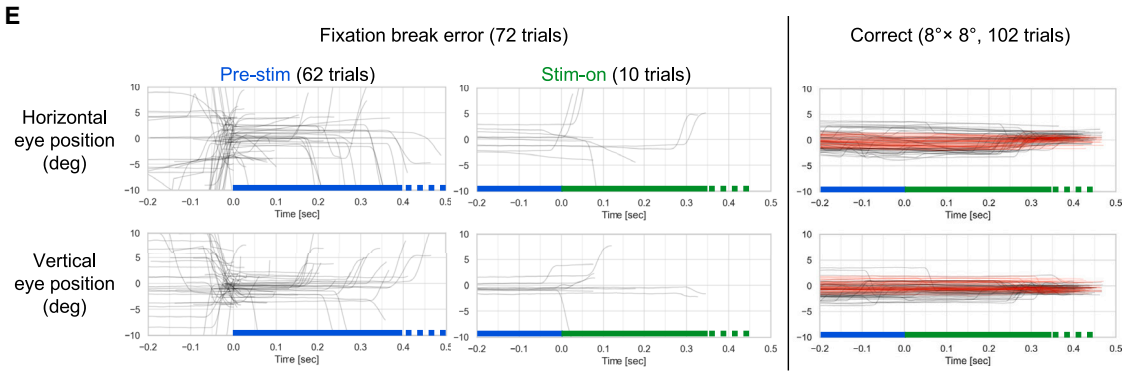

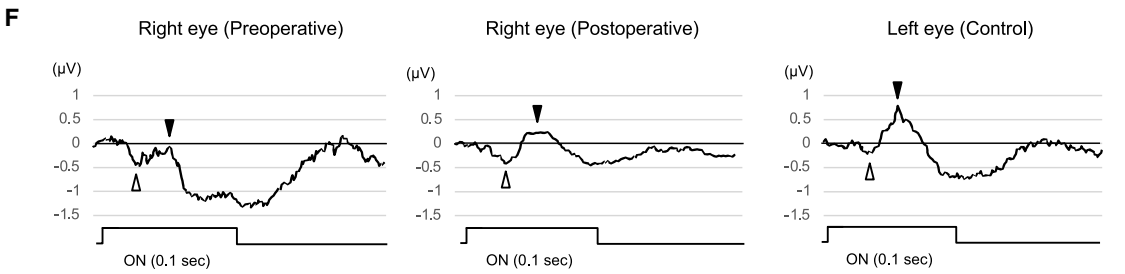

Figure 3. Eye fixation tests and electrophysiological responses of the monkey before and after transplantation

(A and B) Schematic images of test settings (A) and test for one eye (B).

(C) Sequence of events in a trial of the fixation test. Red dots and black-broken-line squares indicate example eye positions of the monkey and the invisible eye windows, respectively.

(D) Correct ratios of the fixation test before and after surgery (4° × 4° eye window). The correct answer ratio was significantly increased on all testing days after surgery. ***$p < 0.0001$, Pearson's chi-squared test against correct/total trials before surgery.

(E) Horizontal (top) and vertical (bottom) eye positions of the right eye across time axis aligned at either the onset of the pre-stim (left panel) or stim-on (middle and right panels) on day 1 (D). Each curve represents data from each trial in which eye positions were within an 8° × 8° eye window. Eye position data were averaged across 10 samples along the time axis and plotted. Red line shows the result of the test using an estimated 4° × 4° eye window.

(F) Focal macular ERGs recorded with a 5°-circle stimulus spot on the right eye (left and middle, preoperative and postoperative ones, respectively) and left eye (right). Pre-stim, pre-stimulus period; Stim-on, stimulus on period; ITI, inter-trial interval.

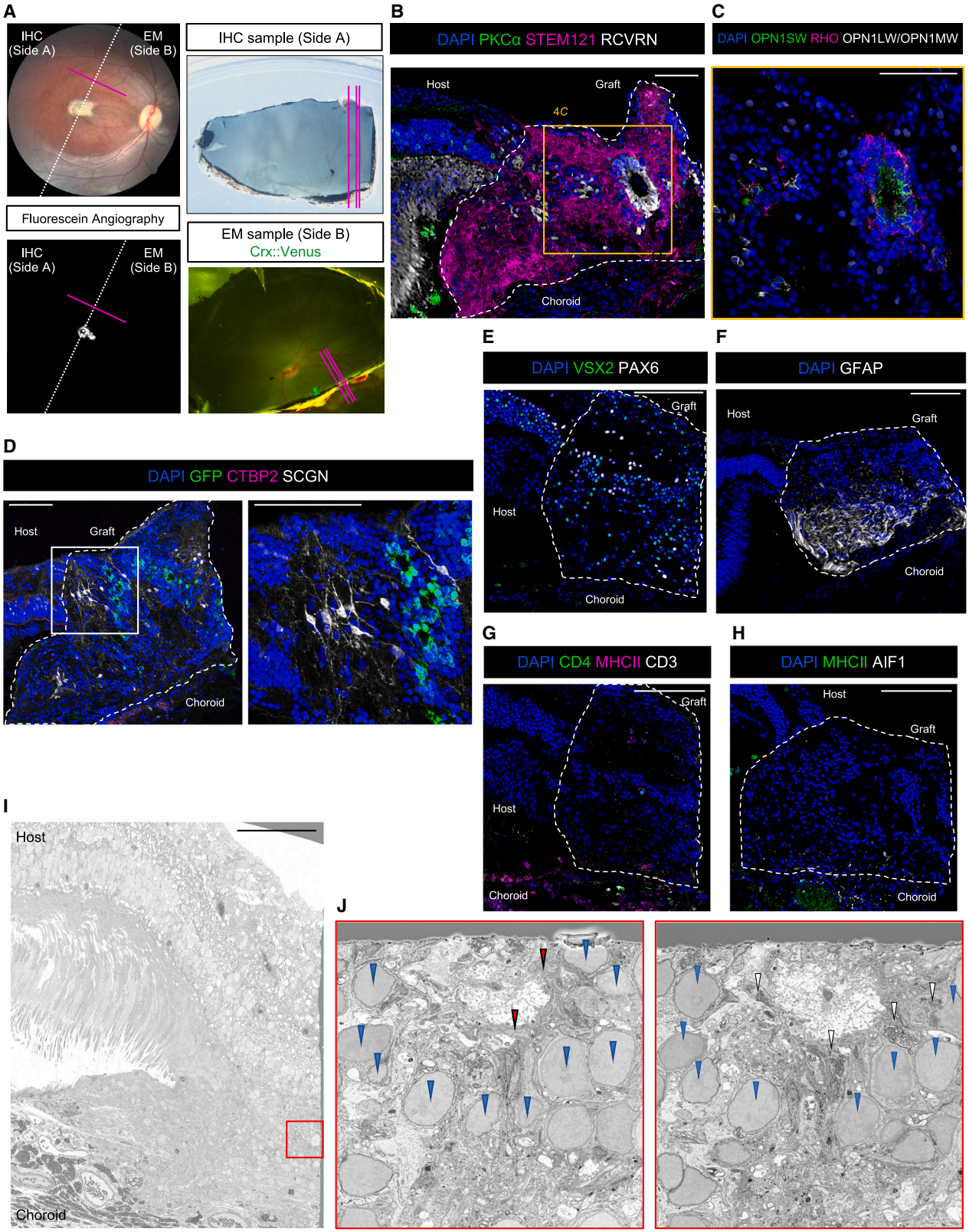

(legend on next page)

host retina and graft status. At approximately 200 days after transplantation (graft DD 259), the transplanted eye (right eye) was harvested and cut into two pieces (sides A and B, respectively, Figure 4A).

In IHC analysis, the human cytoplasm marker STEM121-positive tissue, including PR marker RCVRN-positive cells, continuously fills the host MH space (Figure 4B). Transplanted hESC-derived retina developed rod, L/M-, and S-cone PRs, as indicated by the expression of RHO (rhodopsin), OPN1LW/OPN1MW (L/M-cone opsins), and OPN1SW (S-cone opsin) (Figure 4C). Some SCGN-positive graft cone BPs aligned with the host retina, suggesting a possible interaction with host inner retinal cells such as RGCs or amacrine cells, although this has not been confirmed so far (Figure 4D). Protein kinase C (PKC)α-positive rod BPs were rarely observed within the Islet1$^{-/-}$ graft as previously reported (Figure 4B) (Yamasaki et al., 2022). The graft also includes other retinal interneurons such as VSX2-positive BPs and PAX6-positive amacrine cells, horizontal cells, or RGCs (Figures 4E and S2). Cells positive for activated glial cell marker GFAP were observed in some part of the choroidal side of the graft possibly in response to a mild immune rejection (Figure 4F), because a trace of infiltration of CD4-positive and CD3/CD4-positive T cells was observed in or around the graft (bottom, Figure 4G). Major histocompatibility complex (MHC) II/AIF1-positive activated microglia were not observed in and around the graft (Figure 4H).

We also observed the graft-host retina junction area by EM (see Video S2). The graft PR rosette with mitochondria-rich structures indicated the presence of inner segments (white arrows, Figure 4G). However, well-aligned outer segment discs were not observed, partially due to a mild immune rejection. Synaptic connections were not confirmed with limited EM analysis, where we could not trace all the graft PRs at the host-graft interface.

DISCUSSION

The present MH was associated with ILM peeling and had a moderate size, and thus was not strictly a refractory MH model; however, the post-transplantation course was considered as a mimic for such MHs with PSC-derived RO transplantation. The MH was closed by the seamless integration of the hESC-derived retinal graft that genetically lacks ON-BPs at 7 months after transplantation in the monkey eye. Graft PRs differentiated into rod, L/M-, and S-cone PRs in rosette forms, but we could not confirm the synaptic contact between these PRs and host BPs. The graft cells were not invasive and did not affect the structural alignment of the surrounding host PRs. Although mild immune rejection occurred following the xeno-transplantation, additional focal steroid injection resolved it, and postoperative visual function was subsequently improved in both subjective and objective examinations.

Despite the mild rejection, the grafted retina in this study (graft DD 259) showed a similar potency in PR maturation as those in previous non-human primate studies, but synaptic connections with the host BPs, which was consistently observed in retinal degeneration models, were not confirmed (Shirai et al., 2016; Tu et al., 2019). In retinal transplantation for MHs, the graft PR connectivity requires lateral contact with BPs at the host MH margin that may or may not have been deprived of the host's own PRs. Possible reasons for the lack of synaptic interactions include (1) the period from transplantation to histological examination was too short to evaluate host-graft synapse formation, (2) immune rejection may have caused the formation of secondary gliosis and affected differentiation of some retinal cells in the graft (Figure 4F), and (3) with MH, most host BPs still have partner PRs. Other potential host-graft synaptic connectivities that are not yet studied are the ones between other cell types such as RGCs and

Figure 4. Histological examination of the graft using immunohistochemical and electron microscope analysis

(A) At approximately 200 days after transplantation, the eyeball was cut it into two pieces for IHC (side A) and EM analysis (side B). White dashed lines indicate the cutting line between the IHC and EM samples; each sample was sectioned along the direction of magenta line.

(B–F) IHC images of the graft with low (B, D–F) and high (C and G) magnification on DD60–70. (B) STEM121-positive human grafted tissue (magenta) was present in the host MH space. Rosette structures consisting of RCVRN-positive photoreceptors (PRs, white) were observed in the graft. PKCα-positive rod bipolar cells (BPs, green) were present in the host inner retinal layer but not in the Islet1$^{-/-}$ graft. (C) PRs in the graft expressed RHO (magenta), OPN1LW/OPN1MW (white), and OPN1SW (green). (D) GFP-positive graft PRs (green) consisted of rosette structures, and SCGN-positive cone BPs (white) were observed in the graft. Presynaptic protein marker CtBP2 (magenta, right) well-aligned with the host inner and outer plexiform layers, partly indicating the extent of the host retina. (E) The graft tissue contains VSX2- and PAX6-positive cells (green and white, respectively). (F) The presence of activated glial cell marker GFAP (white) at the host-graft interface is probably related to xenograft rejection responses.

(G and H) CD4-positive T cells (green, G) were observed in the graft, and MHC II-positive macrophages (magenta, G) and CD3/CD4-positive T cells (white/green, G) were observed in the graft-choroid interface. In contrast, MHC II-positive (green, H) activated state AIF1-positive (white, H) microglia were not observed in the graft.

(I and J) EM images of the host-graft interface with low (I) and high (J) magnification. Figure 4I demonstrates the EM analysis on the detailed rosette structure (red square). Blue arrowheads indicate the PR nucleolus composing rosette structures, white contain mitochondria, and red contain external limiting membrane. Scale bars: 100 μm (B–I).

BPs, and also lateral gap junctions between retinal cells in the host and graft.

PSC-derived retinal transplantation partially improved visual function in the refractory MH mimic model animal. Improvement of the b-wave in focal macular ERGs after transplantation (Figure 3F) indicates that the presence of graft tissue positively supported the subsequent recovery of host ON-BP function. These results were consistent with an improvement in eye fixation function after transplantation (Figures 3D and 3E). Interestingly, for L/M- and S-cone opsins, a large number of cone PRs were present in the graft occupying the host MH space after transplantation. Currently, whether transplanted PR precursor cells preferentially differentiated into cones in the foveal environment remains unknown. Further studies will be required to understand how cell composition in the graft influences the visual function.

Using a PSC-derived retinal graft, MH was closed with retinal cells but not by gliosis (Figures 4B–4F), unlike other surgical techniques such as lens capsule, ILM, and amniotic membrane transplantation. The major advantage of our method compared with ART is that it requires no graft harvesting, which may reduce the surgery time and the risks associated with surgical procedures; importantly, this method can spare peripheral visual field defects. Other possible advantages may include the use of PR precursor cells as a major composite of the RO graft, which may potentially enable more efficient host-graft integration compared to mature rod PRs in ART grafts (Assawachananont et al., 2014), and a higher cone content in the PSC-derived RO than that in ART grafts. If cone content can make any difference, further improvement of visual function may be achieved by preparing cone PR-dominant grafts such as by using other differentiation methods (Eldred et al., 2018).

In conclusion, PSC-derived retinal transplantation contributed to MH closure with continuously integrated tissue containing rod, S-, and L/M-cone PRs and improved visual function. This approach simplifies the ART procedure with advantages of (1) no need for harvesting the peripheral retina, (2) preparation of different sizes of sheets, including the one for a large MH, and (3) inclusion of cone PR precursor cells in the graft. Further studies are needed to validate the functional advantage of the PSC-derived retina including the synaptic connectivity with and protective effect for host retinal cells.

EXPERIMENTAL PROCEDURES

Eye fixation test

The monkey was seated in a primate chair in dim light while an eye fixation test was performed. Before this test, the monkey was under step-by-step water restriction for 1 week. In each trial of the eye fixation test, a blue target (0.2° × 0.2°, 9.03 candelas [cd]/m^2) appeared in the center of the screen (Figure 3C, eye-wait; gray background, 30.7 cd/m^2). After the monkey had fixated on the blue target for 0.4–0.5 s (pre-stim), one of the test stimuli was presented for 0.35–0.45 s (stim-on). After disappearance of the test stimulus, a drop of water was delivered as a reward from a drinking spout (Figure 3A). If the monkey broke eye fixation from an invisible eye window (described in the following) during the pre-stim and stim-on periods, an error was registered (left and middle, Figure 3E), and the monkey had to repeat the trial from the beginning with the identical test stimulus. Eye positions were measured using an infrared pupil-position monitoring system (iRecHS2, http://staff.aist.go.jp/k.matsuda/iRecHS2/) (Matsuda et al., 2017). The sizes of the invisible eye windows for the fixation were 4° × 4° and 8° × 8° square (width × height) before and after surgery, respectively, placed at the center of the screen. The behavioral performance post-surgery was adjusted to a window size 4° × 4° *post hoc* (Figure 3D). The fixation test was performed on three days approximately 6 months after transplantation.

In vivo objective ophthalmic examinations

At 1 week before surgery and at 1 and 2 weeks and thereafter every month after surgery, fundus photographs, FA, and FAF images were acquired using a fundus camera (CX-1; Canon), and OCT images using OCT (RS3000; NIDEK). FA images were taken at approximately 1 min (early phase) and 5 min (late phase) after injection of sodium fluorescein. We also performed focal macular ERG tests before and at six months after surgery.

Surgical procedures in retinal transplantation

All surgical procedures were performed by one experienced surgeon (Y.K.) with an OPMI Visu 200 (Carl Zeiss) and a Constellation Vision System (Alcon Laboratories, Inc.). We performed 25-gauge PPV with one 20-gauge infusion port sutured on sclera under general anesthesia for the safe and stable surgical procedure on deep-set macaque eyes with narrow palpebral fissures. A 27-gauge disposable twin light chandelier illuminator (DORC) was used to facilitate bimanual maneuvers. The complete posterior vitreous detachment was induced, and a sticky posterior vitreous cortex on the fovea-parafovea area, suggesting that there was some tangential traction, was removed using a diamond-dusted sweeper (DORC). The ILM was stained with brilliant blue G and gently peeled in the posterior pole area, and the MH was confirmed open by RS3000 (left, Figure 1H).

The sclera was cut with a 23-gauge V-lance ophthalmic knife (MANI, Inc.), and the retinal graft sheet was placed in the posterior pole area using a 24G cannula tip, which was covered by perfluoro-*n*-octane heavy liquid for stable manipulation (Perfluoron; Alcon). The graft edge was grasped with 25-gauge Grieshaber Revolution DSP forceps (MAXGrip and ILM forceps; Alcon) and gently moved toward the MH and flattened at the edge to tuck into the MH space also using a diamond-dusted sweeper (See Video S1). Thereafter, Perfluoron was removed, and the graft position was confirmed using RS3000 (right, Figure 1H). Fluid-air exchange was performed, and all surgical wounds were sutured where necessary.

The procedures for hESC maintenance, retinal differentiation of hESCs and graft preparation, the monkey model, details of eye

fixation test, focal macular ERG recording, monkey sacrifice/eye cup preparation, IHC techniques, and electron microscopy are described in the supplemental experimental procedures.

RESOURCE AVAILABILITY

Lead contact

Further information and requests for resources and reagents should be directed to and will be fulfilled by the corresponding author, Michiko Mandai (e_lab.mandai@kcho.jp).

Materials availability

This study did not generate new unique reagents.

Data and code availability

The raw eye fixation testing data are available on AIST repository (https://aist.repo.nii.ac.jp/records/2003248).

ACKNOWLEDGMENTS

We thank M. Matsumura for her help in cell culture, S. Kitahata and K. Kadonosono for their advice on surgical techniques, R.O.L. Wong and her colleagues for their advice on EM techniques, S. Sugita for his advice on immune response, and M. Kawahara and T. Senba for supporting the animal experiments. We thank Editage (www.editage.jp) for English language editing. Kyoto University provided the human ESC-KhES-1 cell line. This research was supported by the Japan Agency for Medical Research and Development (AMED, grant number JP20bm0204002), the Japan Science and Technology Agency (grant number JPMJMS2022 to S. Yonemura), and the Japan Society for the Promotion of Science (grant number 21H02684 to S. Yonemura).

AUTHOR CONTRIBUTIONS

Conceptualization, Y.I., Y.K., and M.M.; methodology, Y.I., Y.S.-M., Y.K., and M.M.; software, Y.S.-M. and K.M.; formal analysis, Y.I., Y.S.-M., K.M., and M.M.; investigation, Y.I., Y.S.-M., H.U., R.A., K.H., K.M., S. Yokota., Y.K., and M.M.; resources, Y.I., Y.S.-M., K.O., H.U., R.A., T.M., K.H., K.M., S. Yonemura., K.N., M.T., Y.K., and M.M.; data curation, Y.I., Y.S.-M., K.O., and K.M.; writing – original draft, Y.I., Y.S.-M., K.O., and M.M.; writing – review and editing, Y.I. and M.M.; visualization, Y.I., Y.S.-M., K.O., K.M., and S. Yonemura; supervision, K.N., M.T., Y.K., and M.M.; project administration, K.N., M.T., Y.K., and M.M.; funding acquisition, S.Y. and M.T.; all authors reviewed and approved the final manuscript.

DECLARATION OF INTERESTS

The authors declare no competing interests.

SUPPLEMENTAL INFORMATION

Supplemental information can be found online at https://doi.org/10.1016/j.stemcr.2024.09.002.

Received: May 9, 2024
Revised: September 2, 2024
Accepted: September 3, 2024
Published: October 3, 2024

REFERENCES

Assawachananont, J., Mandai, M., Okamoto, S., Yamada, C., Eiraku, M., Yonemura, S., Sasai, Y., and Takahashi, M. (2014). Transplantation of embryonic and induced pluripotent stem cell-derived 3D retinal sheets into retinal degenerative mice. Stem Cell Rep. *2*, 662–674.

Chen, S.N., and Yang, C.M. (2016). Lens capsular flap transplantation in the management of refractory macular hole from multiple etiologies. Retina *36*, 163–170.

Ch'ng, S.W., Patton, N., Ahmed, M., Ivanova, T., Baumann, C., Charles, S., and Jalil, A. (2018). The Manchester Large Macular Hole Study: Is it Time to Reclassify Large Macular Holes? Am. J. Ophthalmol. *195*, 36–42.

Eldred, K.C., Hadyniak, S.E., Hussey, K.A., Brenerman, B., Zhang, P.W., Chamling, X., Sluch, V.M., Welsbie, D.S., Hattar, S., Taylor, J., et al. (2018). Thyroid hormone signaling specifies cone subtypes in human retinal organoids. Science *362*, eaau6348.

Frisina, R., Gius, I., Tozzi, L., and Midena, E. (2022). Refractory full thickness macular hole: current surgical management. Eye *36*, 1344–1354.

Gasparini, S.J., Llonch, S., Borsch, O., and Ader, M. (2019). Transplantation of photoreceptors into the degenerative retina: Current state and future perspectives. Prog. Retin. Eye Res. *69*, 1–37.

Gass, J.D. (1995). Reappraisal of biomicroscopic classification of stages of development of a macular hole. Am. J. Ophthalmol. *119*, 752–759.

Garg, A., Ballios, B.G., and Yan, P. (2022). Spontaneous Closure of an Idiopathic Full-Thickness Macular Hole: A Literature Review. J. Vitreoretin. Dis. *6*, 381–390.

Grewal, D.S., Charles, S., Parolini, B., Kadonosono, K., and Mahmoud, T.H. (2019). Autologous Retinal Transplant for Refractory Macular Holes: Multicenter International Collaborative Study Group. Ophthalmology *126*, 1399–1408.

Hendrickson, A., Possin, D., Vajzovic, L., and Toth, C.A. (2012). Histologic development of the human fovea from midgestation to maturity. Am. J. Ophthalmol. *154*, 767–778.e2.

Mandai, M., Fujii, M., Hashiguchi, T., Sunagawa, G.A., Ito, S.I., Sun, J., Kaneko, J., Sho, J., Yamada, C., and Takahashi, M. (2017). iPSC-Derived Retina Transplants Improve Vision in rd1 End-Stage Retinal-Degeneration Mice. Stem Cell Rep. *8*, 1112–1113.

Matsuda, K., Nagami, T., Sugase, Y., Takemura, A., and Kawano, K. (2017). A Widely Applicable Real-Time Mono/Binocular Eye Tracking System Using a High Frame-Rate Digital Camera. In Human-Computer Interaction, M. Kurosu, ed. (Springer), pp. 593–608.

McCannel, C.A., Ensminger, J.L., Diehl, N.N., and Hodge, D.N. (2009). Population-based incidence of macular holes. Ophthalmology *116*, 1366–1369.

Morgan, I.G., Ohno-Matsui, K., and Saw, S.M. (2012). Myopia. Lancet *379*, 1739–1748.

Lorenzi, U., Mehech, J., Caporossi, T., Romano, M.R., De Fazio, R., Parrat, E., Matonti, F., and Mora, P.; ReMaHo Study Group (2022). A retrospective, multicenter study on the management of macular holes without residual internal limiting membrane: the refractory

macular hole (ReMaHo) study. Graefes Arch. Clin. Exp. Ophthalmol. *260*, 3837–3845.

Morizane, Y., Shiraga, F., Kimura, S., Hosokawa, M., Shiode, Y., Kawata, T., Hosogi, M., Shirakata, Y., and Okanouchi, T. (2014). Autologous transplantation of the internal limiting membrane for refractory macular holes. Am. J. Ophthalmol. *157*, 861–869.e1.

R Development Core Team (2014). R: A Language and Environment for Statistical Computing (R Foundation for Statistical Computing).

Ribeiro, J., Procyk, C.A., West, E.L., O'Hara-Wright, M., Martins, M.F., Khorasani, M.M., Hare, A., Basche, M., Fernando, M., Goh, D., et al. (2021). Restoration of visual function in advanced disease after transplantation of purified human pluripotent stem cell-derived cone photoreceptors. Cell Rep. *35*, 109022.

Rizzo, S., Caporossi, T., Tartaro, R., Finocchio, L., Franco, F., Barca, F., and Giansanti, F. (2019). A Human Amniotic Membrane Plug to Promote Retinal Breaks Repair and Recurrent Macular Hole Closure. Retina *39*, S95–S103.

Shirai, H., Mandai, M., Matsushita, K., Kuwahara, A., Yonemura, S., Nakano, T., Assawachananont, J., Kimura, T., Saito, K., Terasaki, H., et al. (2016). Transplantation of human embryonic stem cell-derived retinal tissue in two primate models of retinal degeneration. Proc. Natl. Acad. Sci. USA *113*, E81–E90.

Singh, M.S., Charbel Issa, P., Butler, R., Martin, C., Lipinski, D.M., Sekaran, S., Barnard, A.R., and Maclaren, R.E. (2013). Reversal of end-stage retinal degeneration and restoration of visual function by photoreceptor transplantation. Proc. Natl. Acad. Sci. USA *110*, 1101–1106.

Spiteri Cornish, K., Lois, N., Scott, N.W., Burr, J., Cook, J., Boachie, C., Tadayoni, R., la Cour, M., Christensen, U., and Kwok, A.K.H. (2014). Vitrectomy with internal limiting membrane peeling versus no peeling for idiopathic full-thickness macular hole. Ophthalmology *121*, 649–655.

Suda, K., Hangai, M., and Yoshimura, N. (2011). Axial length and outcomes of macular hole surgery assessed by spectral-domain optical coherence tomography. Am. J. Ophthalmol. *151*, 118–127.e1.

Tabandeh, H. (2020). Vascularization and Reperfusion of Autologous Retinal Transplant for Giant Macular Holes. JAMA Ophthalmol. *138*, 305–309.

Terasaki, H., Miyake, Y., Tanikawa, A., Kondo, M., Ito, Y., and Horiguchi, M. (1998). Focal macular electroretinograms before and after successful macular hole surgery. Am. J. Ophthalmol. *125*, 204–213.

Tu, H.Y., Watanabe, T., Shirai, H., Yamasaki, S., Kinoshita, M., Matsushita, K., Hashiguchi, T., Onoe, H., Matsuyama, T., Kuwahara, A., et al. (2019). Medium- to long-term survival and functional examination of human iPSC-derived retinas in rat and primate models of retinal degeneration. EBioMedicine *39*, 562–574.

Yamasaki, S., Tu, H.Y., Matsuyama, T., Horiuchi, M., Hashiguchi, T., Sho, J., Kuwahara, A., Kishino, A., Kimura, T., Takahashi, M., and Mandai, M. (2022). A Genetic modification that reduces ON-bipolar cells in hESC-derived retinas enhances functional integration after transplantation. iScience *25*, 103657.